Measurement Report: Abundance and fractional solubilities of aerosol metals in urban Hong Kong: Insights into factors that control aerosol metal dissolution in an urban site in South China

Junwei Yang,[1] Lan Ma,[1] Xiao He,[2] Wing Chi Au,[1] Yanhao Miao,[1] Wen-Xiong Wang,[1,3] Theodora Nah[1,3]*

[1]*School of Energy and Environment, City University of Hong Kong, Hong Kong SAR, China*
[2]*College of Chemistry and Environmental Engineering, Shenzhen University, Shenzhen 518060, China*
[3]*State Key Laboratory of Marine Pollution, City University of Hong Kong, Hong Kong SAR, China*

* To whom correspondence should be addressed: Theodora Nah (Email: theodora.nah@cityu.edu.hk)
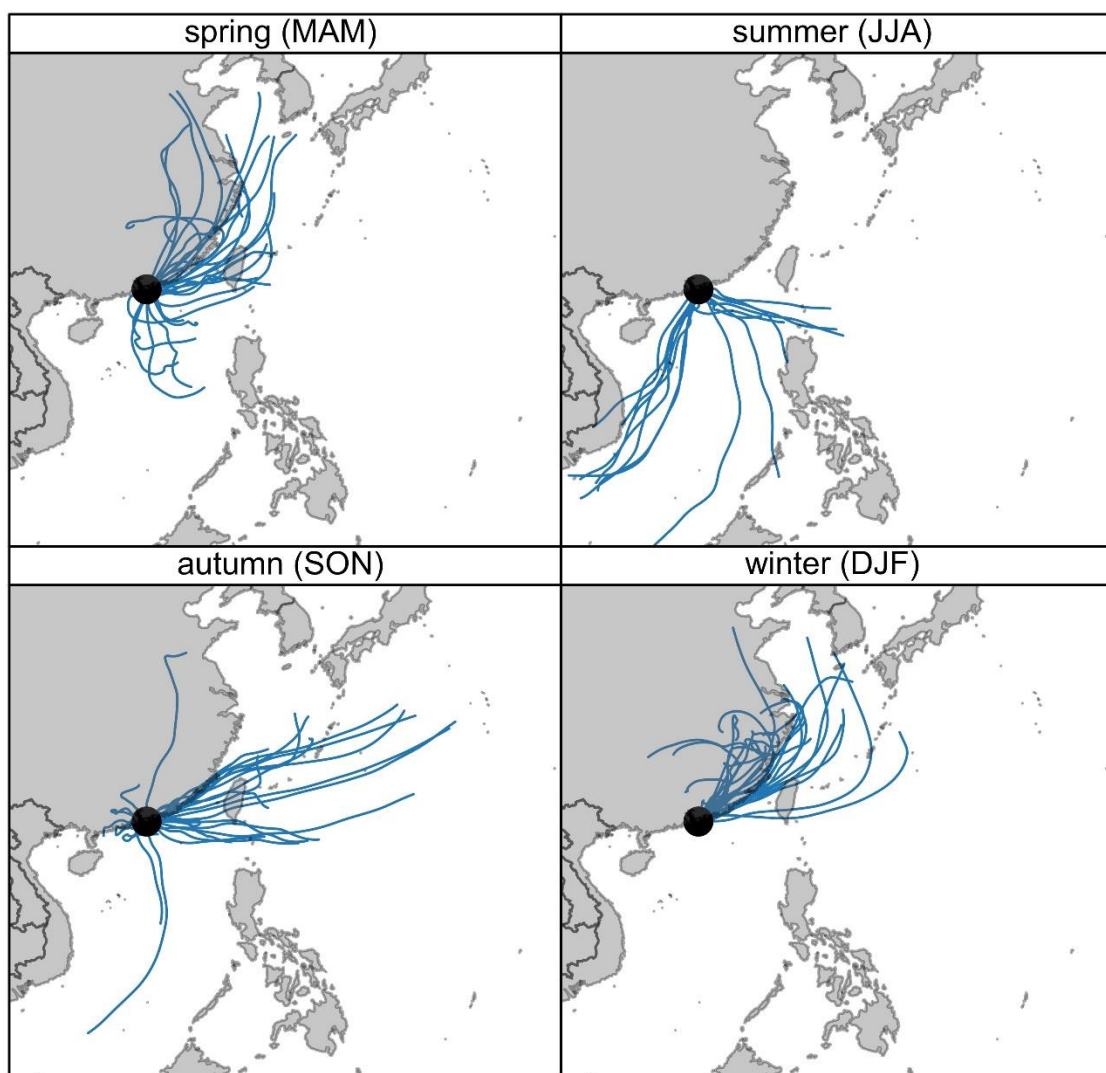
Figure S1: Back trajectories of air masses reaching Hong Kong (latitude = 22.303, longitude = 114.177, height = 100 m, duration = 72 h) during the four sampling periods. Back-trajectories calculations were performed by the Hybrid Split-Particle Lagrangian Integrated Trajectory (HYSPLIT) model using meteorological data from NCEP/NCAR Reanalysis (2.5° latitude-longitude grid).

21
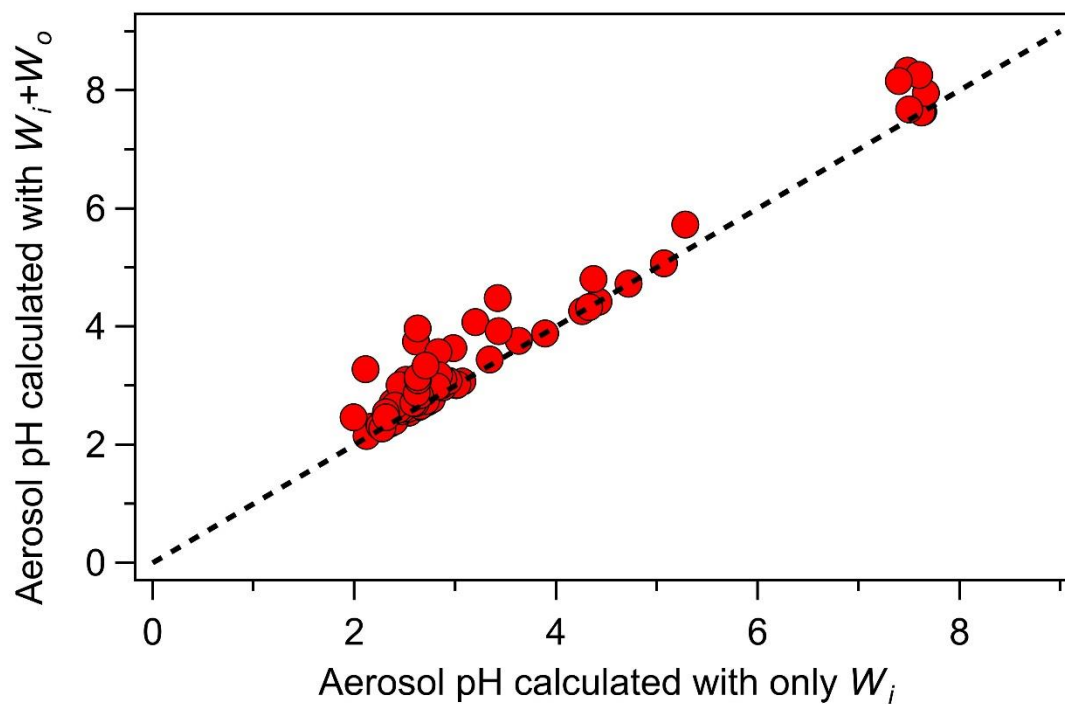
22 **Figure S2:** Comparisons of aerosol pH values calculated with (y axis) vs. without (x axis)

23 contributions from W_o. The dashed line is the 1:1 line. Majority of the predicted pH values lie

24 close to the dashed line. This indicated that the inclusion/exclusion of W_o into calculations

25 did not impact aerosol pH significantly.

26

27
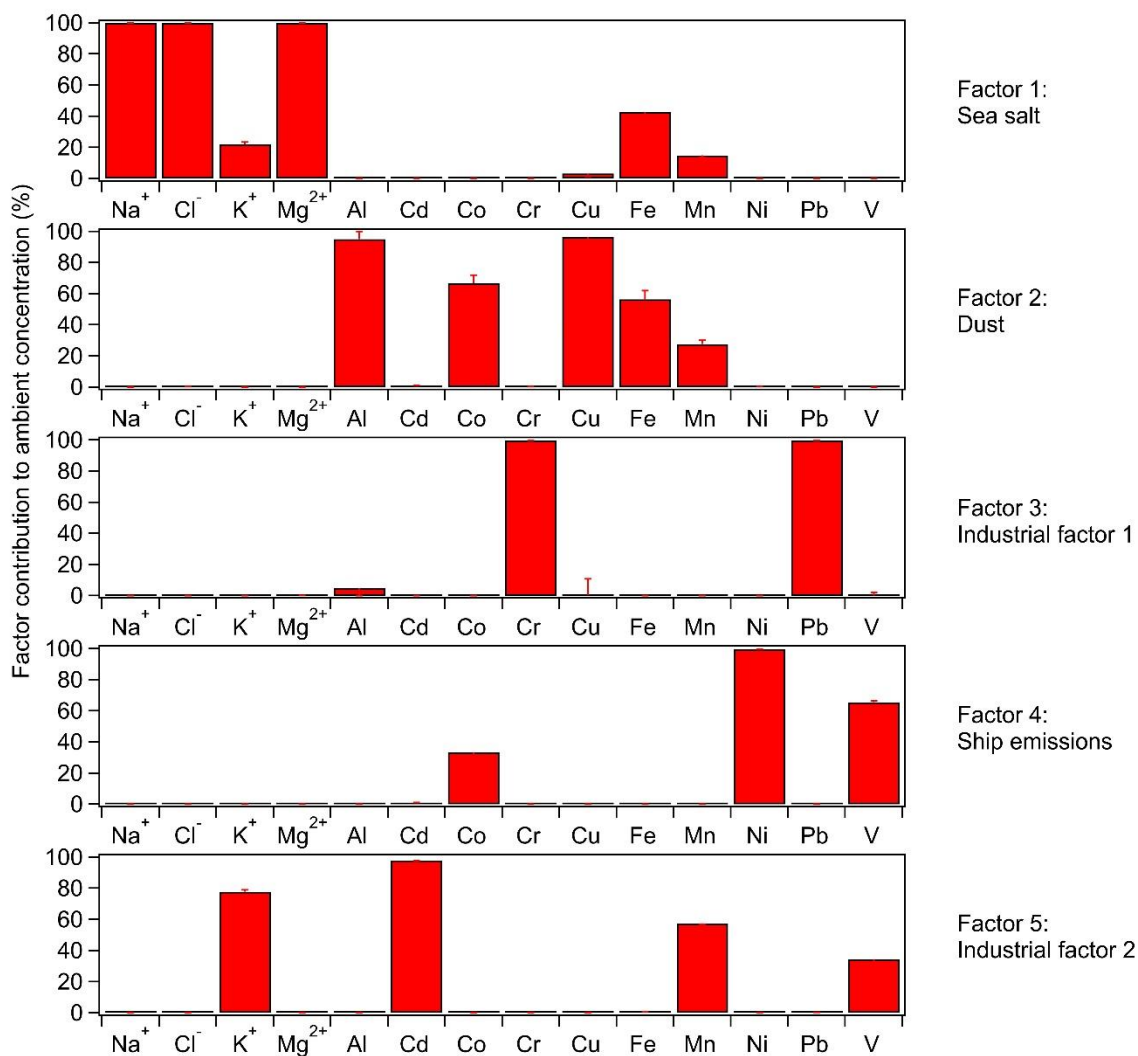
28

29 **Figure S3:** Profiles of the five factors resolved by positive matrix factorization (PMF) using

30 bootstrap (BS) analysis for source apportionment of aerosols measured at the monitoring site.

31 The error bars represent the largest displacement (DISP) uncertainty range from the base run.
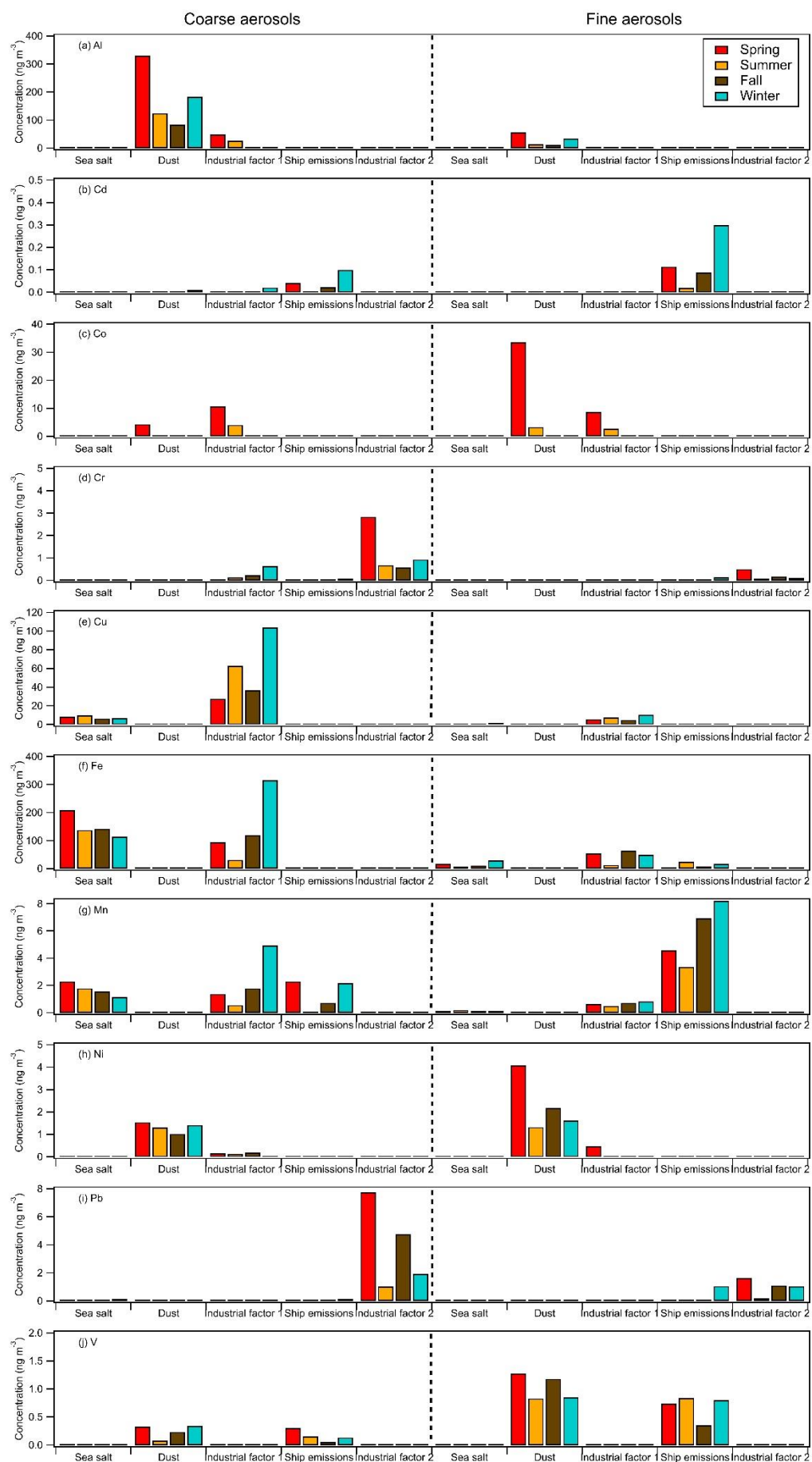
33   **Figure S4:** Seasonal mass contributions of each source to each species in coarse and fine

34   aerosols.

35
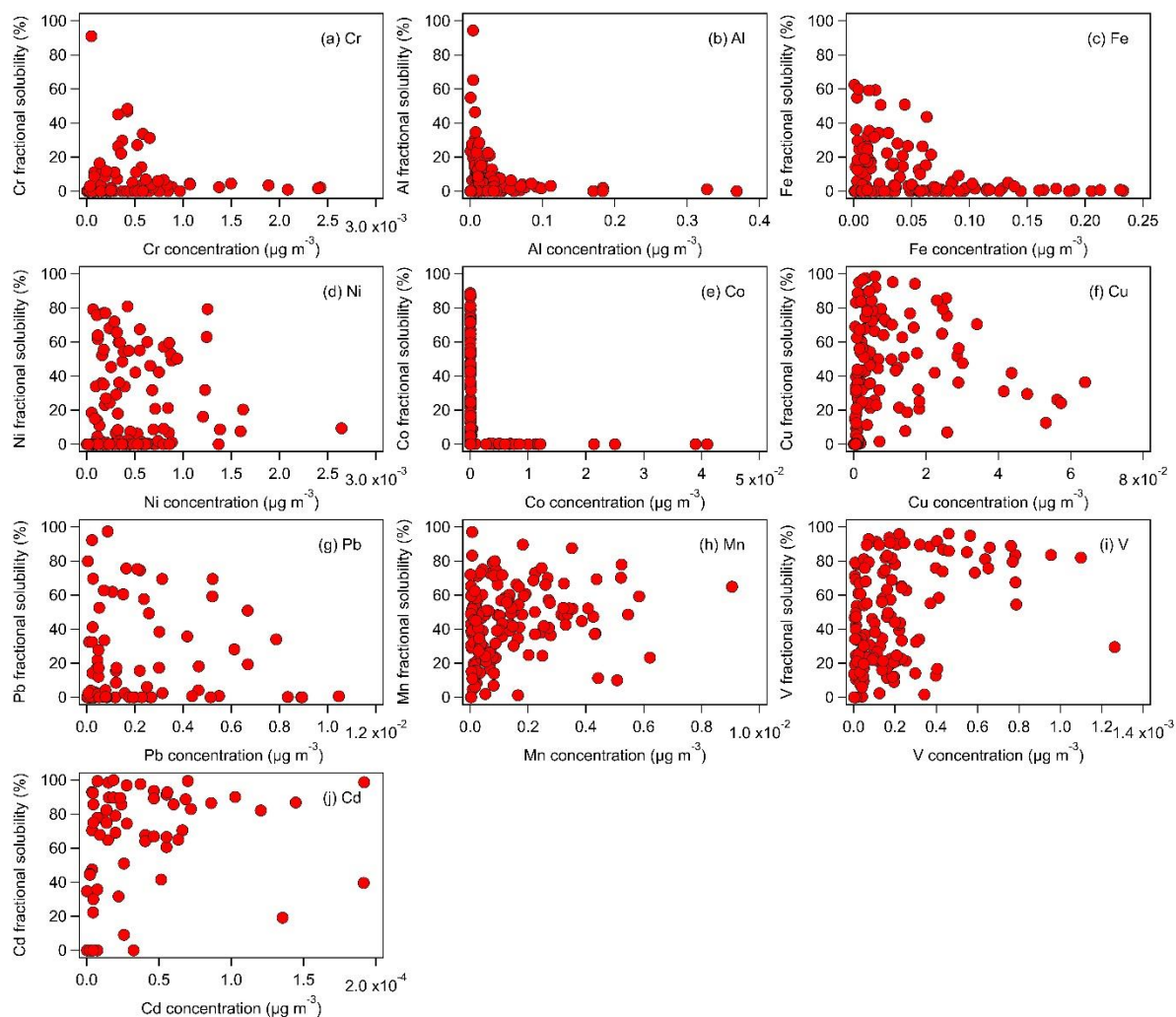
36   **Figure S5:** Metal fractional solubility vs. total metal concentration for fine and coarse aerosols.

37   The fractional solubility values were calculated by dividing the water-soluble metal mass

38   concentration by the total metal mass concentration. Only data with non-zero total metal

39   concentrations were used in the figures.

40
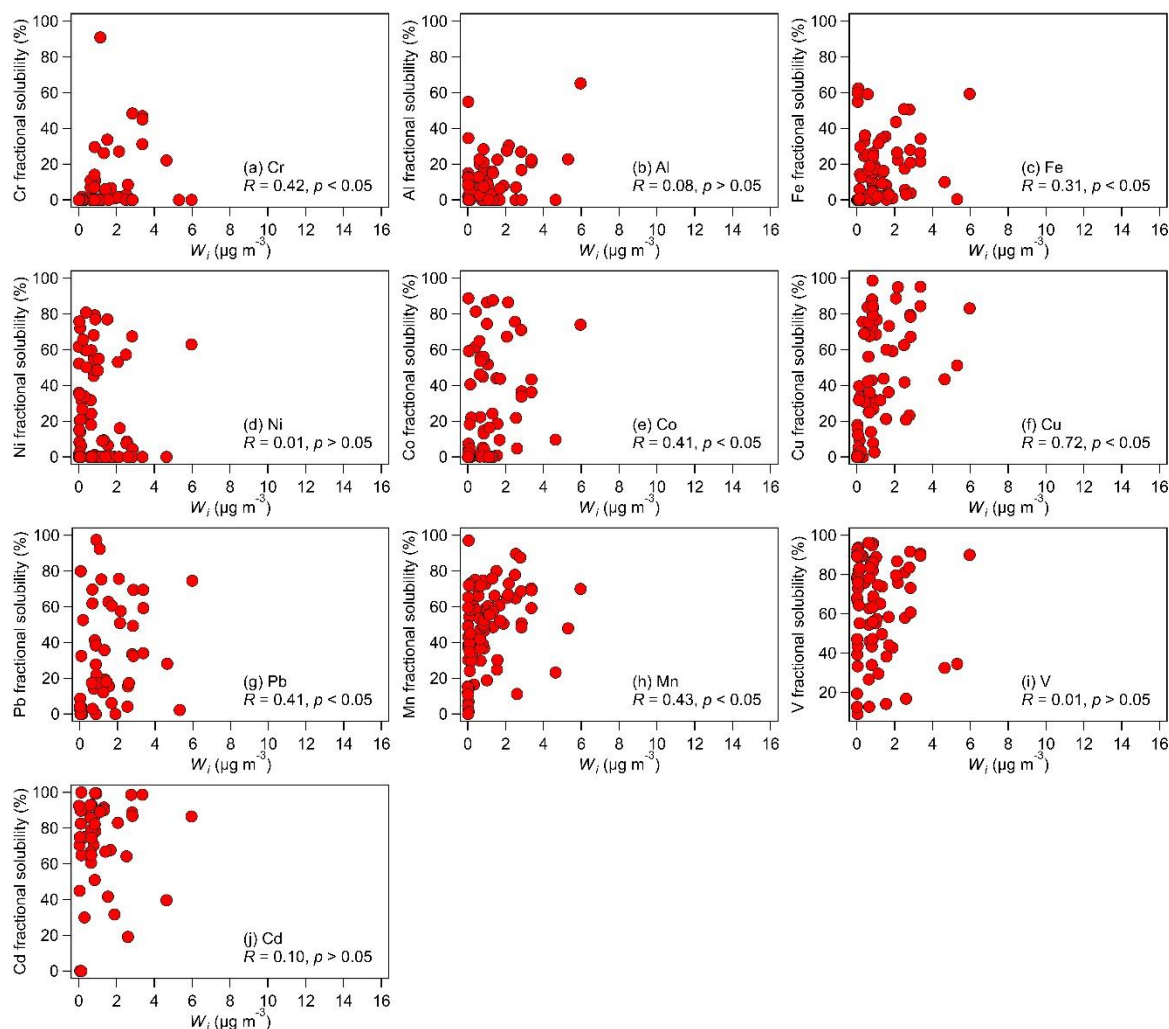
Figure S6: Relationships between the metal fractional solubilities and W_i in fine aerosols. Only data with non-zero total metal concentrations were used in the figures. Also shown are the spearman correlation coefficients for each relationship.

44
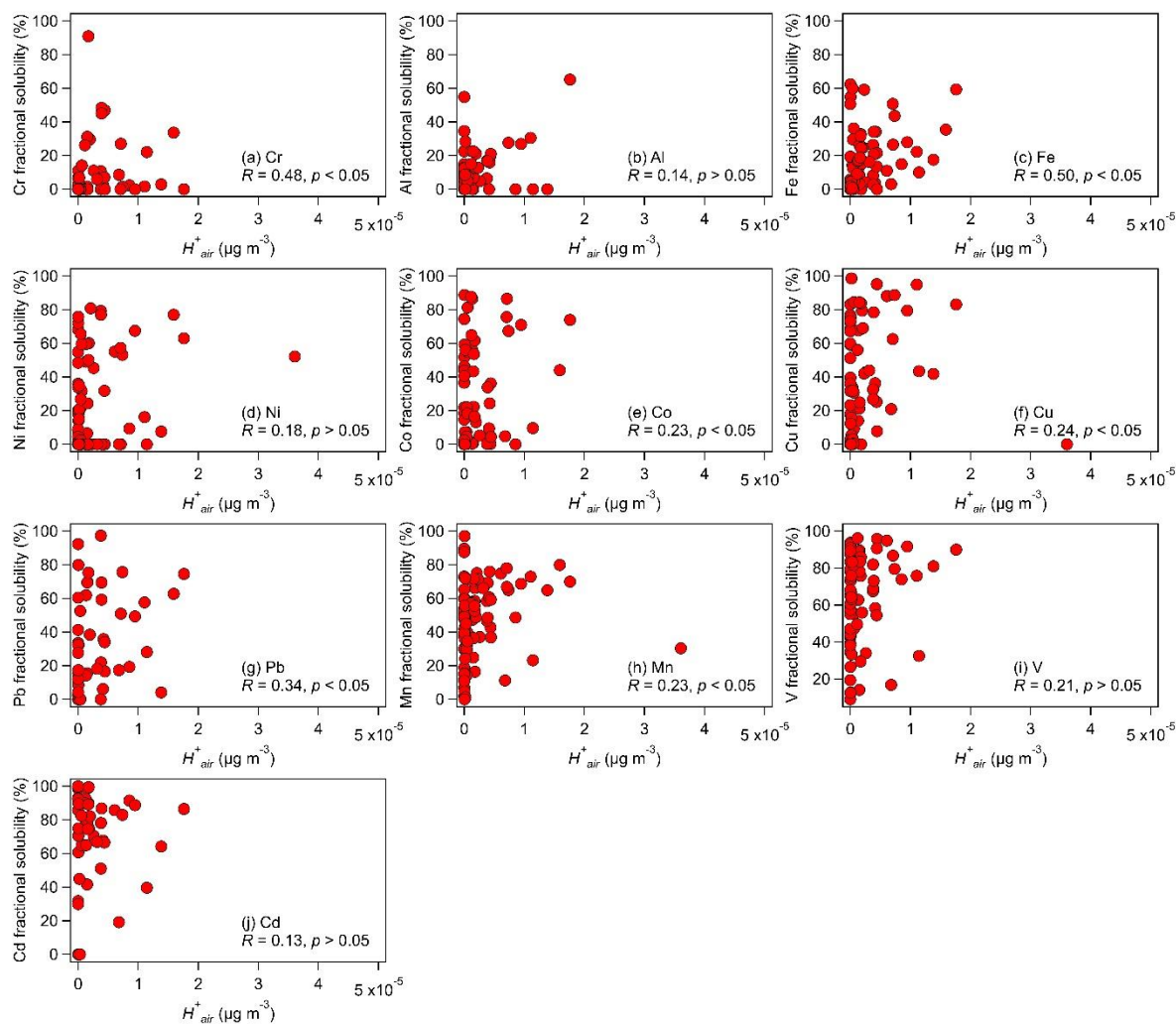
Figure S7: Relationships between the metal fractional solubilities and H^+_{air} in fine aerosols.
Only data with non-zero total metal concentrations were used in the figures. Also shown are
the spearman correlation coefficients for each relationship.

48
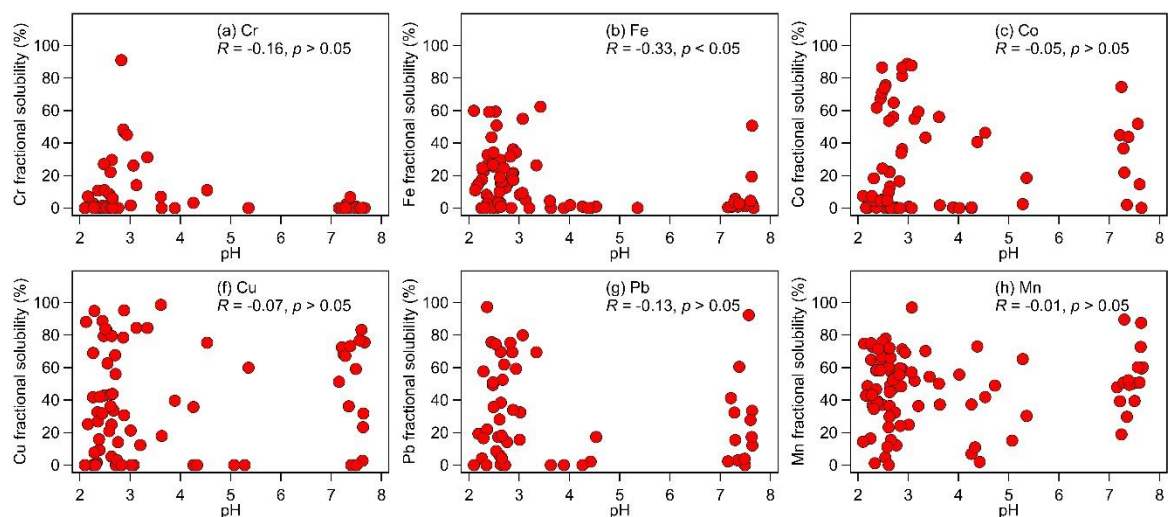
Figure S8: Relationships between the Cr, Fe, Co, Cu, Pb, and Mn fractional solubilities and fine aerosol pH. Only data with non-zero total metal concentrations were used in the figures. Also shown are the spearman correlation coefficients for each relationship. Only the correlation between the Fe fractional solubility and fine aerosol pH was statistically significant.

66   **Table S1:** Comparison of average total metal concentrations (ng m^{-3}) in 2012/2013 by Jiang et

67   al. (2015) and 2021/2022 (this study) at a Kowloon Tong in Hong Kong

68   (a) Comparison of winter mass concentrations

Metal	Jiang et al. (2015)[a]		This study[b]	
	Fine	Coarse[c]	Fine	Coarse[c]
Cr	3	2.7	0.68	1.66
Al	254	301.2	47.54	184.67
Fe	137	142	95.70	432.04
Ni	4.4	1.6	1.63	1.43
Cu	19.7	4	10.06	106.92
Pb	49.4	2.9	8.52	2.06
Mn	17.1	5.2	9.20	8.25
V	9.2	0.9	1.25	0.48
Cd	1.1	0.1	0.18	0.06

69   [a] Measurements were performed from 12 November 2012 to 10 December 2012.

70   [b] Measurements were performed from 15 December 2021 to 26 January 2022.

71   [c] Mass concentrations measured for the MOUDI impactor stage 11 (18 µm nominal cutoff) was

72   excluded in this comparison since Jiang et al. (2015) reported mass concentrations for PM$_{2.5-10}$

73   for their coarse aerosol measurements.

74

75   (b) Comparison of spring/summer mass concentrations

Metal	Jiang et al. (2015)[a]		This study[b]	
	Fine	Coarse[c]	Fine	Coarse[c]
Cr	7.2	1.5	1.86	2.15
Al	591	528.9	60.47	302.70
Fe	190.6	153	66.11	259.24
Ni	10	1.3	3.40	1.60
Cu	21.6	5.5	7.30	39.94
Pb	52.7	2.8	6.27	5.20
Mn	19.3	5	4.82	4.66
V	25.6	1.8	1.72	0.50
Cd	1.2	0.1	0.07	0.02

76   [a] Measurements were performed from 8 April 2013 to 13 May 2013.

77   [b] Measurements were performed from 7 March 2021 to 4 April 2021, 23 to 30 June 2021, and

78   7 to 14 July 2021.

79   [c] Mass concentrations measured for the MOUDI impactor stage 11 (18 µm nominal cutoff) was

80   excluded in this comparison since Jiang et al. (2015) reported mass concentrations for PM$_{2.5-10}$

81   for their coarse aerosol measurements.

82

83 **Table S2:** Spearman rank correlations between the water-soluble and total metals in fine and

84 coarse aerosols[a]

Metal	Fine	Coarse
Cr	**0.49**	**0.50**
Al	**0.40**	0.14
Fe	**0.58**	**0.48**
Ni	**0.43**	**0.30**
Co	0.16	0.06
Cu	**0.86**	**0.81**
Pb	**0.60**	**0.43**
Mn	**0.93**	**0.95**
V	**0.89**	**0.81**
Cd	**0.96**	**0.64**

85 [a] Bold: statistically significant ($p < 0.05$)

86

87

88

89

90

91

92

93

94

95

96

97

98

Section S1. Source apportionment

To identify the major sources of the measured total aerosol metals, source apportionment was performed with positive matrix factorization (PMF) using EPA PMF 5.0 software. PMF decomposes the measured concentration matrix (x_{ij}) into two matrices: the factor contributions matrix (g_{ik}) and factor profiles (f_{kj}) plus a residue matrix (e_{ij}) (Paatero and Tapper, 1994; Paatero, 1997):

$$x_{ij} = \sum_{k=1}^{p} g_{ik}f_{kj} + e_{ij} \cdots \qquad (1)$$

where p is the number of factors determined by the user. Factor contributions and profiles are determined by minimizing the objective function (Q):

$$Q = \sum_{i=1}^{n} \sum_{j=1}^{m} \left[\frac{x_{ij} - \sum_{k=1}^{p} g_{ik}f_{kj}}{u_{ij}} \right]^2 \cdots \qquad (2)$$

where u_{ij} is the uncertainty matrix provide by the user. The ultimate goal is to achieve chemical mass balance between the measured species and source contributions by minimizing Q. Two error estimation approaches were used to analyze the model-resolved factor profiles: Bootstrap (BS) and Displacement (DISP) (Paatero et al., 2014). The EPA PMF 5.0 software conducts BS by randomly perturbing the original data set and generating new PMF results using the resampled version of input data. The BS factor is subsequently assigned to the base run factor with which the BS factor has the highest correlation, above a user-defined threshold. BS estimation involves uncertainties derived from random errors and partially from rotational ambiguity. The EPA PMF 5.0 software performs DISP by "displacing" each variable in the well-fitted factor f_{kj} far enough such that Q increases by a pre-defined maximum value dQ^{max}. Such extensions estimate the upper and lower intervals of each species in the factor profile. By nature, DISP reflects the uncertainty derived from rotational ambiguity.

The mass concentrations of 14 chemical species (Na$^+$, Cl$^-$, K$^+$, Mg^{2+}, ^{27}Al, ^{51}V, ^{52}Cr, ^{55}Mn, ^{57}Fe, ^{59}Co, ^{60}Ni, ^{65}Cu, ^{111}Cd, and ^{208}Pb) measured on each MOUDI stage during every sampling period (total of 175 sets of samples) were used as the input matrix. 100 BS runs were performed. Uncertainties were as following:

$$u_{ij} = \sqrt{(x_{ij} \times EF)^2 + (MDL)^2} \cdots \qquad (3)$$

where x_{ij} is the measured concentration, EF is the user-defined error fraction for individual species derived from the experimental data, and MDL is the method detection limit. For concentrations below MDL, the uncertainty was set to 5/6 × MDL. In PMF, the optimal number of factors is a compromise between resolving factors with the best physical meanings and a good fit for all input species. 3 to 7 factors were tested, and the final number was determined by examining the changes in Q_{robust}/Q_{exp} and the physical interpretation of each factor. $Q_{exp} \approx nm - p(n+m)$, denotes the degree of freedom of the model solution, where n, m, and p refer to the number of samples, the number of species input into PMF, and the number of factors. Based on the minimal Q values and the physical interpretations of the resolved factor, the five-factor solution was selected. These five factors were broadly classified as: Sea salt, Dust, Industrial, Residual oil, and Ship emissions. The Q_{robust}/Q_{exp} changed 14.8% from a four-factor to a five-factor solution, while the Q_{robust}/Q_{exp} changed 22.6% from a three-factor solution to a four-factor solution.

Figure S3 shows the factor profiles resolved in the five-factor solution. Source identification was based on the tracer species with the highest mass loadings. The first factor was marked by the high loadings of common sea salt tracers Na^+, Cl^-, and Mg^{2+}, thus it was identified as "sea salt" (Chow et al., 2022). The second factor was identified as "dust" due to its high loadings of Al, Fe, and Mn, which are known mineral dust tracers (Chow et al., 2022). Cu is also a dominant species in this second factor. Previous studies have attributed Cu to brake/tire wear, and Fe and Mn to both dust and brake/tire wear (Garg et al., 2000; Adachi and Tainosho, 2004; Lough et al., 2005). Thus, resuspended road dust containing brake/tire wear particles could have contributed to this "dust" factor. The fourth factor was identified as "ship emissions" since it was marked by high loadings of Ni and V, which are known tracers for ship emissions (Chow et al., 2022). The third and fifth factors were broadly classified as "industrial factor 1" and "industrial factor 2" since their dominant metal species are typically associated with industrial emissions (Chow et al., 2022).

Section S2. Aerosol liquid water concentration associated with organics

The following equation was used to calculated the aerosol liquid water concentration (μg m^{-3}) associated with organic species (Guo et al., 2015):

$$W_o = \frac{m_{org}\rho_w}{\rho_{org}} \frac{\kappa_{org}}{(\frac{1}{RH}-1)} \tag{4}$$

where m_{org} is the organic mass concentration (μg m^{-3}), ρ_w is the water density (1 μg m^{-3}), ρ_{org} is the organic density, k_{org} is the organic hygroscopicity parameter, and RH is the relative humidity of the sampling period. We calculated m_{org} by multiplying the measured water-soluble organic carbon (WSOC) concentration by 1.6, which is the conversion factor recommended for converting WSOC to organic mass in urban aerosols (Turpin and Lim, 2001). We assumed ρ_{org} to be 1.4 g cm^{-3}, which is the value usually assumed for the density of ambient organic aerosols in previous studies (Guo et al., 2015; Shiraiwa et al., 2017; Kuwata et al., 2012; King et al., 2007). We used 0.35 for κ_{org}, which is the average of the range of values (0.28 to 0.39) previously measured for organic aerosols in Hong Kong (Meng et al., 2014).

References

Adachi, K. and Tainosho, Y.: Characterization of heavy metal particles embedded in tire dust, Environment International, 30, 1009-1017, https://doi.org/10.1016/j.envint.2004.04.004, 2004.

Chow, W. S., Huang, X. H. H., Leung, K. F., Huang, L., Wu, X., and Yu, J. Z.: Molecular and elemental marker-based source apportionment of fine particulate matter at six sites in Hong Kong, China, Science of The Total Environment, 813, 152652, https://doi.org/10.1016/j.scitotenv.2021.152652, 2022.

Garg, B. D., Cadle, S. H., Mulawa, P. A., Groblicki, P. J., Laroo, C., and Parr, G. A.: Brake Wear Particulate Matter Emissions, Environmental Science & Technology, 34, 4463-4469, https://doi.org/10.1021/es001108h, 2000.

Guo, H., Xu, L., Bougiatioti, A., Cerully, K. M., Capps, S. L., Hite Jr, J. R., Carlton, A. G., Lee, S. H., Bergin, M. H., Ng, N. L., Nenes, A., and Weber, R. J.: Fine-particle water and pH in the southeastern United States, Atmos. Chem. Phys., 15, 5211-5228, https://doi.org/10.5194/acp-15-5211-2015, 2015.

Jiang, S. Y., Kaul, D. S., Yang, F., Sun, L., and Ning, Z.: Source apportionment and water solubility of metals in size segregated particles in urban environments, Science of The Total Environment, 533, 347-355, https://doi.org/10.1016/j.scitotenv.2015.06.146, 2015.

King, S. M., Rosenoern, T., Shilling, J. E., Chen, Q., and Martin, S. T.: Cloud condensation nucleus activity of secondary organic aerosol particles mixed with sulfate, Geophysical Research Letters, 34, https://doi.org/10.1029/2007GL030390, 2007.

Kuwata, M., Zorn, S. R., and Martin, S. T.: Using elemental ratios to predict the density of organic material composed of carbon, hydrogen, and oxygen, Environ Sci Technol, 46, 787-794, https://doi.org/10.1021/es202525q, 2012.

Lough, G. C., Schauer, J. J., Park, J.-S., Shafer, M. M., DeMinter, J. T., and Weinstein, J. P.: Emissions of Metals Associated with Motor Vehicle Roadways, Environmental Science & Technology, 39, 826-836, https://doi.org/10.1021/es048715f, 2005.

Meng, J. W., Yeung, M. C., Li, Y. J., Lee, B. Y. L., and Chan, C. K.: Size-resolved cloud condensation nuclei (CCN) activity and closure analysis at the HKUST Supersite in Hong Kong, Atmos. Chem. Phys., 14, 10267-10282, https://doi.org/10.5194/acp-14-10267-2014, 2014.

Paatero, P.: Least squares formulation of robust non-negative factor analysis, Chemometrics and Intelligent Laboratory Systems, 37, 23-35, https://doi.org/10.1016/S0169-7439(96)00044-5, 1997.

Paatero, P. and Tapper, U.: Positive matrix factorization: A non-negative factor model with optimal utilization of error estimates of data values, Environmetrics, 5, 111-126, https://doi.org/10.1002/env.3170050203, 1994.

Paatero, P., Eberly, S., Brown, S. G., and Norris, G. A.: Methods for estimating uncertainty in factor analytic solutions, Atmos Meas Tech, 7, 781-797, 10.5194/amt-7-781-2014, 2014.

Shiraiwa, M., Li, Y., Tsimpidi, A. P., Karydis, V. A., Berkemeier, T., Pandis, S. N., Lelieveld, J., Koop, T., and Pöschl, U.: Global distribution of particle phase state in atmospheric secondary organic aerosols, Nature Communications, 8, 15002, https://doi.org/10.1038/ncomms15002, 2017.

Turpin, B. J. and Lim, H.-J.: Species Contributions to PM2.5 Mass Concentrations: Revisiting Common Assumptions for Estimating Organic Mass, Aerosol Science and Technology, 35, 602-610, https://doi.org/10.1080/02786820119445, 2001.